Theoretical Study of the Q and B Bands of Free-Base, Magnesium, and Zinc Porphyrins, and Their Derivatives

ARTICLE *in* THE JOURNAL OF PHYSICAL CHEMISTRY A · MARCH 1999

Impact Factor: 2.69 · DOI: 10.1021/jp984807d

4 AUTHORS, INCLUDING:

Yoong-Kee Choe

National Institute of Advanced Industrial Sci…

36 PUBLICATIONS **686** CITATIONS

SEE PROFILE

Theoretical Study of the Q and B Bands of Free-Base, Magnesium, and Zinc Porphyrins, and Their Derivatives

Tomohiro Hashimoto, Yoong-Kee Choe, Haruyuki Nakano, and Kimihiko Hirao*

Department of Applied Chemistry, Graduate School of Engineering, The University of Tokyo, Tokyo 113-8656, Japan

Received: December 29, 1998; In Final Form: January 19, 1999

The multireference Møller−Plesset perturbation (MRMP) theory with complete active space self-consistent field (CASSCF) reference functions is applied to the study of the Q and B bands of free-base, magnesium, and zinc porphyrins and their derivatives. The Q band of free-base porphyrin is so weak because the transition is pseudoparity-forbidden because of the alternancy symmetry. The Q band in the visible region can be intensified if the pairing property is broken. This is achieved by various chemical modifications to the basic structure of free-base porphyrin such as external substituents, changes in conjugation pathway, and change in central substituent. The intensity and color of the Q band as well as the macrocyclic porphyrin skeleton are perturbed to a greater or lesser extent by various chemical modifications. Insertion of aza groups in meso position leads to the shrinking of the size of the central hole, whereas hydrogenation to the exo double bond of pyrrole rings expands the central hole. Substitution of nitrogen atoms for meso carbon atoms significantly intensifies the oscillator strength of the higher energy side transition of the Q band with the peak position unchanged. Ring reduction widens the splitting of two peaks of the Q band, giving rise to the characteristically strong far-red band and the weaker visible band. Changes from metal-free to metalloporphyrins have a less dramatic effect on the spectra.

1. Introduction

Porphyrins and their derivatives play an important role in the biochemistry of all living systems. They form the backbone of pigments such as chlorophyll and heme, which have a universal biological distribution and were involved in the oldest metabolic phenomena on earth. Thus, knowledge of these systems and their excited states is essential in understanding a wide variety of biological processes, including oxygen binding, electron transfer, catalysis, and the initial photochemical step in photosynthesis.

It was recognized early that the intensity and color of porphyrins are derived from the highly conjugated π-electron systems. The electronic spectra of porphyrin compounds are characterized by three basic regions. The so-called Q band is relatively weak and occurs in the visible region. The Q band consists of a degenerate electronic transition for divalent metalloporphyrins and two separate electronic transitions for free-base porphyrins (FBP). The intense Soret or B band occurs in the near-UV and is often accompanied by a closely related N band of lower intensity. The B band for divalent metalloporphyrins is assumed to be a degenerate pair. The higher UV bands in the third region are broad and are often of near uniform intensity.

The absorption spectrum of porphyrins has long been understood in terms of the highly successful "four-orbital" (two highest occupied π orbitals and two lowest unoccupied π^* orbitals) model first applied by Gouterman.[1] This picture, although oversimplified, well reproduces the major feature of these systems. The Q and B bands arise from a linear combination of these one-electron transitions. For the lower Q band, the transition dipoles nearly cancel giving rise to the relatively weak absorption in the visible region. For the higher energy B band, the transition dipoles reinforce, resulting in the very intense absorption in the UV region.

FBP is assumed to be the 18 π-electron conjugated system. Gouterman's four orbitals correspond to the highest occupied molecular orbital (HOMO), next HOMO, lowest unoccupied molecular orbital (LUMO), and next LUMO of naphthacene which is also the 18 π-electron polyacene as shown in Figure 1. Naphthacene is a typical alternant hydrocarbon and the pairing properties are satisfied.[2] Let the HOMO (a_u), next HOMO (b_{1u}), LUMO (b_{2g}), and next LUMO (b_{3g}) of alternant hydrocarbon be designated by 1, 2, 1′, and 2′, respectively. The (1,1′) and (2,2′) are called a conjugated pair of orbitals. Because of the pairing property the energy of the configuration obtained by exciting an electron from the orbital i to the orbital j′ is equal to that obtained by excitation from j to i′. The linear combinations of the two degenerate configurations generate the minus (−) and plus (+) states. The minus state is a covalent state whereas the plus state is an ionic state both for singlet and triplet states, which stems from the character of the states in a valence bond description. The HOMO→LUMO (1→1′) excitation gives rise to the lowest $^1B_{2u}{}^+$ state with the ionic nature. The two single excitations of 1→2′ and 2→1′ result in a pair of covalent $^1B_{3u}{}^-$ and ionic $^1B_{3u}{}^+$ states. The electric dipole transition moment vectors for the one-electron i→j′ and j→i′ ($i \neq j$) transitions are similar in magnitude and parallel in their orientation in the alternant hydrocarbons. For i→i′ transitions, the dipole transition moment vector for 1→1′ is antiparallel to that for 2→2′. Thus, the transition to $^1B_{3u}{}^-$ is pseudoparity-forbidden, whereas transitions to $^1B_{2u}{}^+$ and $^1B_{3u}{}^+$ are dipole-allowed.

* Corresponding author. E-mail: hirao@qcl.t.u-tokyo.ac.jp.

10.1021/jp984807d CCC: $18.00
Published on Web 03/09/1999

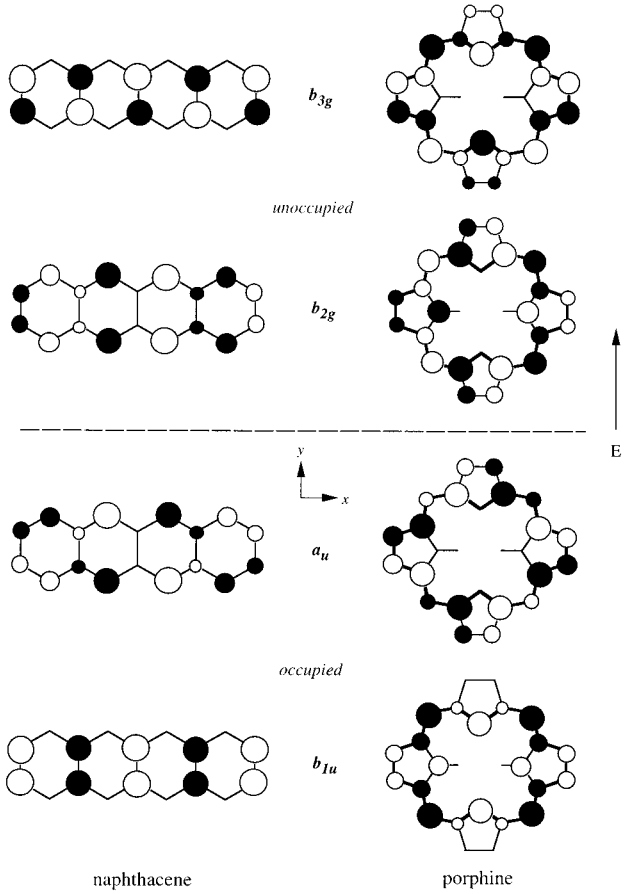

Figure 1. HOMO (a_u), next HOMO (b_{1u}), LUMO (b_{2g}), and next LUMO (b_{3g}) orbitals of free-base porphyrin and naphthacene.

Porphyrins are analogues of alternant hydrocarbons and the above-mentioned pairing properties are satisfied to a great extent. The ground state of FBP is the 1^1A_g state and the transition to the Q band is dipole-allowed. The weakness of the Q band is not due to the degeneracy of orbitals but is due to the alternancy symmetry. The transitions which give rise to the lower component of the Q band ($^1B_{3u}$) are $a_u \rightarrow b_{3g}$ ($1 \rightarrow 2'$) and $b_{1u} \rightarrow b_{2g}$($2 \rightarrow 1'$) and they mix with a different sign. These transition dipole moment vectors are almost the same in magnitude and parallel in their orientation, leading to the cancelation of their intensities. A similar cancelation also occurs in the upper component (1^1B_{2u}) which has the main transitions of $a_u \rightarrow b_{2g}$ ($1 \rightarrow 1'$) and $b_{1u} \rightarrow b_{3g}$($2 \rightarrow 2'$).

The Q band of FBP is weak because the transitions are psuedoparity-forbidden as a result of the alternancy symmetry; thus, one can increase intensity of the absorption in visible region by breaking the pseudoparity. This can be achieved by various chemical modifications to the basic structure of FBP: (1) external substituents, (2) changes in conjugation pathway, and (3) change in central substituent.

A variety of compounds are known in which the macrocyclic porphyrin skeleton is retained, while one or more of the exo double bonds of pyrrole rings are removed. These compounds are formally derived from porphyrins by hydrogenation and are, therefore, commonly termed hydroporphyrins. As shown in Figure 1, a conjugated pair of orbitals of $a_u(1)$ and $b_{2g}(l')$ has amplitude at the peripheral carbons of the pyrrole rings. Thus, a_u and b_{2g} orbitals are expected to be destabilized going from FBP to hydroporphyrins and the alternancy symmetry is not retained in hydroporphyrins. We expect, therefore, the increase of the intensity of the Q band in hydroporphyrins because the cancelation of transition moment vectors is incomplete.

In addition to external substitution, it is known that porphyrin spectra are affected by changes in the path of conjugation. The typical example is the tetrabenzoporphyrin obtained by fusing benzo rings on the four pyrroles. This perturbation to the conjugated ring electrons causes a major change in the optical spectrum. Insertion of aza groups in the inner 16-membered ring, such as fusion of a benzo rings onto the pyrrole, produces major optical effects. Because the nitrogen is more electronegative than the carbon, the three $b_{1u}(2)$, $b_{2g}(l')$, $b_{3g}(2')$ orbitals with the significant amplitude at the methine bridge carbons are expected to be stabilized going from FBP to azaporphyrins. However, the $a_u(1)$ orbital has little amplitude at the methine bridge and therefore it is rather insensitive to the insertion of aza groups. Again, the alternancy symmetry is not retained in tetraazaporphyrin (TA-P) and the increase of the Q band intensity is expected.

From the early days of study it was known that free-base porphyrin with two hydrogens in the center has a four-banded visible spectrum distinctly different from the two-banded visible spectrum shown by most metal complexes and by the acid dication. This is a reflection of the molecular symmetry. The molecular symmetry shifts from rectangular D_{2h} to square D_{4h} in going from FBP to metalloporphyrins. The b_{2g} and b_{3g} orbitals in the D_{4h} metalloporphyrins are enforced to be degenerate because of the 4-fold axes.

In the present paper, we study systematically the excited states (Q and B bands) of FBP, Mg-porphyrin (Mg-P), and Zn-porphyrin (Zn-P) and their substituted analogues. The porphyrins treated in this study are listed in Figure 2. The porphyrin reduced by hydrogenation of one of the pyrrole rings is known as chlorin, the parent of the chlorophyll systems, but we use the notation of dihydroporphyrin (DH-P) for this molecule here. Porphyrin with opposite pyrrole rings reduced, bacteriochlorin, a parent of the bacteriochlorophyll systems, is referred to here as tetrahydroporphyrin (TH-P). To determine the enhanced effects of external substituents and changes in conjugation pathway, we also study tetrahydro, tetraazaporphyrin (TH,TA-P). We investigate the intensity variations and wavelength shifts of the Q and B bands caused by the various chemical modifications.

2. Computational Details

The molecules are placed in the *xy*-plane. The inner hydrogen−hydrogen axis of FBP is set to the *x*-axis. The molecular structure is optimized at the Hartree−Fock (HF) level for the closed-shell ground state of each molecule. The self-consistent field (SCF) approximation artificially favors frozen resonance structures with alternating single and double bonds rather than the delocalized structures for porphyrins.[3] Thus, the SCF calculations are restricted HF and constrained to high symmetry. Excited states are calculated at the optimized geometry, thus we computed vertical excitation energies. The basis set used was (9s4p)/[2s2p] for carbon and nitrogen atoms and (4s)/[ls] for hydrogen atoms. The primitives are cited from Dunning's cc-pVDZ basis set.[4] For Mg and Zn atoms, Huzinaga's (11s5p) and (13s7p5d) sets[5] are contracted to [4s2p] and [5s3p2d], respectively.

First, we carried out the state-averaged complete active space self-consistent field (CASSCF) calculations.[6] The ground state and four valence $\pi-\pi^*$ excited states were averaged with eight π electrons distributed among eight π orbitals (four occupied π orbitals and four unoccupied π^* orbitals). For DH-P, we averaged seven lowest states. These active orbitals are selected so as to form a conjugated pair of orbitals and they belong to b_{1u}, b_{2g}, b_{3g}, and a_u irreducible representations of the D_{2h}

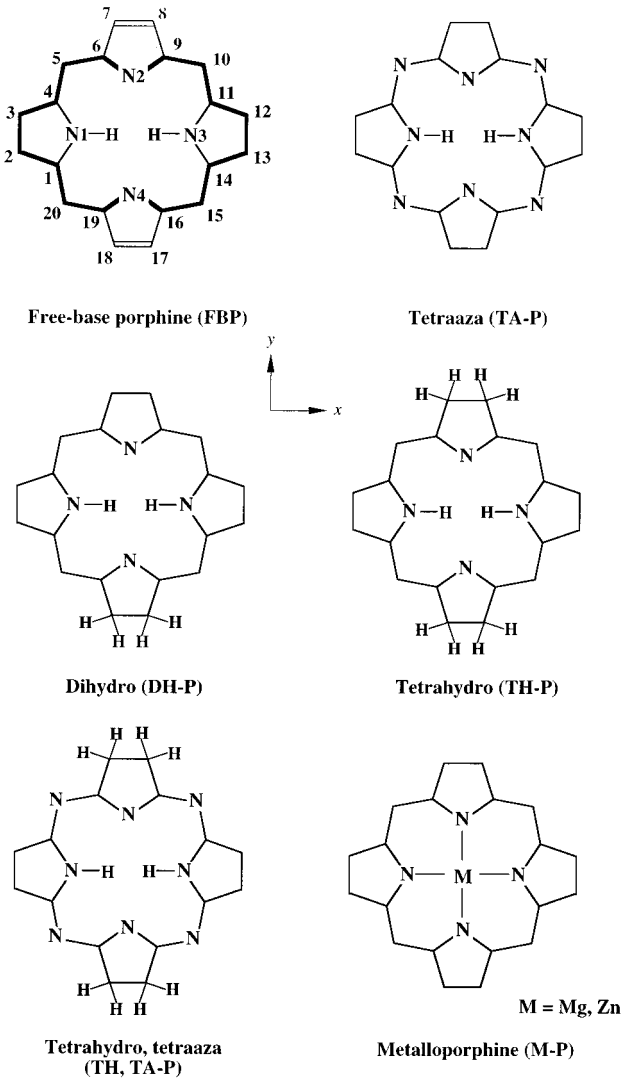

Figure 2. Structural formula of metal-free porphyrins and metalloporphyrins treated in this study. Free-base porphyrin also illustrates the position of atoms used in Table 1.

symmetry. Then the second-order multireference Møller−Plesset perturbation (MRMP)[7] procedure was applied to each individual state to introduce dynamic $\sigma-\pi$ polarization effects. Oscillator strengths were calculated using the CASSCF transition dipole moments and the MRMP transition energies.

3. Results and Discussion

Molecular Structures. The structures of FBP, Mg-P, and Zn-P and their derivatives are optimized at the SCF level. FBP has two hydrogen atoms bonded to pyrrole nitrogen atoms, fixing the two hydrogen atoms on opposite nitrogen atoms. There are small differences in geometry of the two distinct types of five-membered rings in FBP. Table 1 shows selected bond distances and angles for the two types of five-membered rings of FBP and their derivatives. The atomic labeling is shown in Figure 1. Ring 1 (R1) has a hydrogen atom bonded to nitrogen whereas ring 2 (R2) does not. Experimental data[8] are also listed in parentheses for comparison.

Calculated bond lengths and bond angles of FBP show a good agreement with experiment. The deviations from experiment are −0.01 to +0.02 Å in the C_{meso}—C bond and −0.005 to −0.03 Å in the N—C bond, where minus means the underestimation. The maximum deviation is found in the nitrogen and inner hydrogen bond. The computed value of 1.028 Å is longer by 0.16 Å than experiment. The distance of inner hydrogen atoms is calculated to be 2.107 Å. This large discrepancy suggests that the experimental value[8] may be affected by the tautomeric shifts of the two hydrogen atoms among the four nitrogen atoms. Previous MP2[3] and density functional theory[9] also computed the N—H bond to be ca. 1.03 Å.

There are small differences in the geometry of the two distinct types of five-membered rings in FBP. The diagonal N—N separations are nearly equivalent, with N_1—N_3 = 4.163 Å and N_2—N_4 = 4.060 Å. The polygon defined by four nitrogen atoms is thus diamond-shaped. Insertion of aza groups in meso position changes the structure considerably. The calculated N_{meso}—C bonds for TA-P are 0.06−0.07 Å shorter than the corresponding C_{meso}—C bonds for FBP and also the methine bridge angle becomes smaller by 3°, causing the size of the central hole to shrink. The diagonal N—N separations are N_1—N_3 = 3.955 Å and N_2—N_4 = 3.830 Å, which are about 0.2 Å shorter than the corresponding N—N distances of FBP. As a result, the distance of inner hydrogen atoms is reduced to 1.907 Å.

Hydrogenation to the exo double bond of pyrrole rings leads to the opposite effect. Each derivative has the reduced pyrrole ring and the C—C single bond distance is calculated to be 1.513−1.530 Å. Because of the considerable elongation of the exo C—C bond, both the methine bridge angle and the C—N—C angle in the pyrrole ring increase, leading to enlargement of the central hole in hydroporphyrins. For example, the diagonal N—N separations in TH-P become N_1—N_3 = 4.154 Å and N_2—N_4 = 4.250 Å. The N_2—N_4 distance is elongated by 0.2 Å more than the corresponding distance of FBP, whereas the N_1—N_3 separation remains similar to that of FBP. The N_2—N_4 distance becomes longer than the N_1—N_3 distance. Thus, the orientation of the diamond shape formed by four nitrogen atoms switches in going from FBP to TH-P.

The effects of two different perturbations, insertion of aza groups and hydrogenation, are reflected on the structure variations of DH-P and TH,TA-P. The N_2—N_4 separation in DH-P is slightly more elongated than that of FBP, whereas there is little change in the N_1—N_3 separation. In TH,TA-P, the size of the central hole becomes smaller as in TA-P but the direction of the diamond shape is opposite to that of FBP and TA-P.

The calculated geometrical parameters of Mg-P and Zn-P and their derivatives are given in Tables 1(b) and (c). We see that there is little difference in geometrical changes between metal-free and metalloporphyrins. There is also little difference between Mg-P and Zn-P. Thus, the Mg and Zn substitution has much less effect on the deformation than the insertion of aza groups and hydrogenation. Although the size of the central hole of the metalloporphyins is very similar to that of FBP, hydrogenation to Mg-P tends to expand the central hole and the insertion of aza groups shrinks the hole slightly. The diamond shape defined by four nitrogen atoms of metalloporphyrins has the same tendency as that for metal-free porphyrins.

As shown above, the porphyrin skeleton is considerably perturbed because of the chemical modifications. Note that the size of the central hole increases in the order of TA-P < TH,TA-P < FBP < DH-P < TH-P. This relative order is retained even for the metalloporphyrins.

The Q and B Bands of Metal-Free Porphyrins. First we will discuss the electronic structure of FBP. The electronic feature of porphyrin is the 18-membered ring with 18 π electrons, including four nitrogen atoms directed toward the

TABLE 1: Optimized Bond Lengths (Å) and Bond Angles (degree) for the Ground State at the SCF Level[a]

(a) free-base porphyrins

length and angle	FBP	TA-P	TH-P	TH,TA-P	DH-P
N1−1 (R1)	1.369 (1.377−1.383)	1.368	1.372	1.372	1.350
N4−19 (R2)	1.358 (1.363−1.389)	1.357	1.344	1.345	1.349
1−2 (R1)	1.428 (1.425−1.437)	1.440	1.422	1.431	1.435
18−19 (R2)	1.456 (1.439−1.465)	1.464	1.517	1.513	1.516
N1−4 (R1)	1.369 (1.377−1.383)	1.368	1.372	1.372	1.391
17−18 (R2)	1.346 (1.344−1.346)	1.344	1.530	1.528	1.526
1−20	1.380 (1.378−1.398)	1.309	1.386	1.316	1.395
19−20	1.384 (1.374−1.382)	1.321	1.377	1.311	1.372
N1−N3	4.163	3.955	4.154	3.941	4.162
N2−N4	4.060	3.830	4.250	4.006	4.135
N1−H_i	1.028 (0.86)	1.024	1.023	1.019	1.026
N4−19−18 (R2)	110.3 (109.3−110.4)	110.6	111.8	112.2	112.0
N2−6−7 (R2)	110.3 (109.3−110.4)	110.6	111.8	112.2	110.7
6−N2−9 (R2)	106.3 (105.9−106.3)	106.0	110.5	109.8	105.9
17−18-19 (R2)	106.5 (106.1−108.4)	106.4	102.9	102.9	103.0
6−7−8 (R2)	106.5 (106.1−108.4)	106.4	102.9	102.9	106.4
16−N4−19 (R2)	106.3 (105.9−106.3)	106.0	110.5	109.8	110.0
N1−1−20 (R1)	126.1 (124.8−125.8)	127.4	126.3	127.4	126.9
N1−4−5 (R1)	126.1 (124.8−125.8)	127.4	126.3	127.4	125.8
N4−19−20 (R2)	125.7 (124.1−125.6)	127.1	126.1	127.3	126.5
5−6−N2 (R2)	125.7 (124.1−125.6)	127.1	126.1	127.3	125.1
1−20−19	126.6 (126.5−127.7)	123.8	128.2	125.4	127.0
4−5−6	126.6 (126.5−127.7)	123.8	128.2	125.4	127.4
1−N1−H_i	124.7 (120.3−130.2)	124.8	124.6	124.7	125.8
4−N1−H_i	124.7 (120.3−130.2)	124.8	124.6	124.7	123.5

(b) Mg-porphyrins

length and angle	Mg-P	Mg-TA-P	Mg-TH-P	Mg-TH,TA-P	Mg-DH-P
N1−1 (R1)	1.366	1.362	1.369	1.365	1.335
N4−19 (R2)	1.366	1.362	1.352	1.352	1.365
1−2 (R1)	1.443	1.455	1.432	1.443	1.449
18−19 (R2)	1.443	1.455	1.515	1.515	1.515
N1−4 (R1)	1.366	1.362	1.369	1.365	1.401
17−18 (R2)	1.354	1.353	1.530	1.533	1.526
1−20	1.386	1.323	1.393	1.331	1.414
19−20	1.386	1.323	1.372	1.308	1.359
N1−N3	4.103	3.953	4.067	3.940	4.102
N2−N4	4.103	3.953	4.250	4.070	4.151
Mg−N1	2.052	1.976	2.034	1.970	2.051
Mg−N2	2.052	1.976	2.125	2.035	2.062
Mg−N4	2.052	1.976	2.125	2.035	2.089
N4−19−18 (R2)	108.9	108.2	110.9	110.2	110.8
N2−6−7 (R2)	108.9	108.2	110.9	110.2	109.7
6−N2−9 (R2)	107.8	109.1	111.5	112.4	106.9
17−18−19 (R2)	107.2	107.3	103.4	103.6	103.8
6−7−8 (R2)	107.2	107.3	103.4	103.6	106.8
16−N4−19 (R2)	107.8	109.1	111.5	112.4	110.9
N1−1−20 (R1)	125.6	127.0	126.0	126.9	125.8
N1−4−5 (R1)	125.6	127.0	126.0	126.9	125.8
N4−19−20 (R2)	125.6	127.0	125.8	127.5	126.7
5−6−N2 (R2)	125.6	127.0	125.8	127.5	124.5
1−20−19	126.6	125.0	127.5	126.0	126.4
4−5−6	126.6	125.0	127.5	126.0	127.4
1−N1−Mg	126.1	125.5	126.4	125.8	126.9
4−N1−Mg	126.1	125.5	126.4	125.8	125.4
19−N4−Mg	126.1	125.5	124.2	123.8	124.5

(c) Zn-porphyrins

length and angle	Zn-P	Zn-TA-P	Zn-TH-P	Zn-TH,TA-P	Zn-DH-P
N1−1 (R1)	1.365	1.361	1.370	1.365	1.336
N4−19 (R2)	1.365	1.361	1.349	1.350	1.363
1−2 (R1)	1.443	1.456	1.431	1.443	1.449
18−19 (R2)	1.443	1.456	1.515	1.515	1.514
N1−4 (R1)	1.365	1.361	1.370	1.365	1.399
17−18 (R2)	1.353	1.352	1.530	1.533	1.326
1−20	1.385	1.322	1.391	1.330	1.411
19−20	1.385	1.322	1.370	1.308	1.359
N1−N3	4.094	3.954	4.020	3.915	4.083
N2−N4	4.094	3.954	4.276	4.093	4.151
Zn−N1	2.047	1.977	2.010	1.958	2.042

TABLE 1 (Continued)

(c) Zn-porphyrins

length and angle	Zn-P	Zn-TA-P	Zn-TH-P	Zn-TH,TA-P	Zn-DH-P
Zn−N2	2.047	1.977	2.138	2.046	2.058
Zn−N4	2.047	1.977	2.138	2.046	2.093
N4−19−18 (R2)	108.9	108.2	110.8	110.2	110.7
N2−6−7 (R2)	108.9	108.2	110.8	110.2	109.7
6−N2−9 (R2)	107.8	109.0	111.5	112.3	107.0
17−18−19 (R2)	107.2	107.3	103.5	103.6	103.8
6−7−8 (R2)	107.2	107.3	103.5	103.6	106.8
16−N4−19 (R2)	107.8	109.0	111.5	112.3	111.0
N1−1−20 (R1)	125.5	127.0	125.5	126.5	125.5
N1−4−5 (R1)	125.5	127.0	125.5	126.5	125.6
N4−19−20 (R2)	125.5	127.0	126.2	127.7	126.8
5−6−N2 (R2)	125.5	127.0	126.2	127.7	124.5
1−20−19	126.8	125.0	127.7	126.1	126.5
4−5−6	126.8	125.0	127.7	126.1	127.7
1−N1−Zn	126.1	125.5	126.3	125.8	126.8
4−N1−Zn	126.1	125.5	126.3	125.8	125.5
19−N4−Zn	126.1	125.5	124.2	123.8	124.5

[a] See Figure 1 for atomic labeling. Values in parentheses of FBP are experimental values; ref 8. H_i in Table(a) indicates an inner hydrogen. R1 and R2 are the pyrrole rings with and without bonded inner hydrogen, respectively.

TABLE 2: Main Configurations in CASSCF(8e,8o) Wave Functions of the Q Band of Porphyrins

		type of transitions			
state	compound	$b_{1u} \rightarrow b_{2g}$	$a_u \rightarrow b_{3g}$	$b_{1u} \rightarrow b_{3g}$	$a_u \rightarrow b_{2g}$
		free-base porphyrins			
1^1B_{3u}	TA-P	0.512	−0.768	−	−
	FBP	0.653	−0.650	−	−
	DH-P[a]	0.585	−0.693	−	−
	TH-P	0.449	−0.801	−	−
	TH,TA-P	0.352	−0.848	−	−
1^1B_{2u}	TA-P	−	−	0.455	0.818
	FBP	−	−	0.628	0.699
	DH-P[b]	−	−	0.642	0.621
	TH-P	−	−	0.742	0.577
	TH,TA-P	−	−	0.578	0.734
		Mg-porphyrins			
1^1B_{3u}	Mg-TA-P	0.462	−0.806	−	−
	Mg-P	0.628	−0.687	−	−
	Mg-DH-P[a]	0.481	−0.792	−	−
	Mg-TH-P	0.369	−0.847	−	−
	Mg-TH,TA-P	0.292	−0.876	−	−
1^1B_{2u}	Mg-TA-P	−	−	0.462	0.807
	Mg-P	−	−	0.628	0.687
	Mg-DH-P[b]	−	−	0.692	0.551
	Mg-TH-P	−	−	0.742	0.561
	Mg-TH,TA-P	−	−	0.583	0.719
		Zn-porphyrins			
1^1B_{3u}	Zn-TA-P	0.456	−0.809	−	−
	Zn-P	0.624	−0.690	−	−
	Zn-DH-P[a]	0.480	−0.793	−	−
	Zn-TH-P	0.372	−0.845	−	−
	Zn-TH,TA-P	0.293	−0.875	−	−
1^1B_{2u}	Zn-TA-P	−	−	0.456	0.809
	Zn-P	−	−	0.624	0.690
	Zn-DH-P[b]	−	−	0.689	0.556
	Zn-TH-P	−	−	0.738	0.568
	Zn-TH,TA-P	−	−	0.574	0.727

[a] 1^1B_2 state with C_{2v} symmetry. Type of transitions are $a_2 \rightarrow b_1$ and $b_1 \rightarrow a_2$. [b] 2^1A_1 state with C_{2v} symmetry. Type of transitions are $a_2 \rightarrow a_2$ and $b_1 \rightarrow b_1$.

center. This electronic structure is responsible for porphyrin-type optical spectra.

The CASSCF configurations for the low-lying valence $\pi \rightarrow \pi^*$ excited states are given in Table 2. The ground state is well-described by the HF configuration. The ground state is of a covalent character. The energy was computed to be −984.74782 au at the MRMP level. Calculated vertical excitation energies and oscillator strengths of the metal-free porphyrins are summarized in Table 3(a) with the experimental data[10−15] available. Previous ab initio calculations[11,16−20] are also listed for comparison.

The lowest singlet excited state is computed to be the l^1B_{3u}. Table 2 shows that the 1^1B_{3u} state is well-described by singly excited $\pi \rightarrow \pi^*$ configurations of $1 \rightarrow 2'$ and $2 \rightarrow 1'$, which have nearly the same weight with a different sign. The pairing property is fully satisfied at the CASSCF level. The 1^1B_{3u} state is a covalent minus state. MRMP predicts that it appears at 1.63 eV, which is slightly underestimated compared to the experimental value of 1.98−2.02 eV, observed in the gas-phase energy-loss spectrum.[10] SAC-CI,[19] CASPT2,[18] and STEOM-CCSD[20] give 1.75, 1.63, and 1.75 eV for the transition, respectively. The electric transition dipole moment vectors for $1 \rightarrow 2'$ and $2 \rightarrow 1'$ transitions are similar in magnitude and parallel in their orientation. Thus, the transition dipoles nearly cancel in the 1^1B_{3u} state giving rise to the weak absorption in the visible region. The computed oscillator strength of 0.0026 is very low as expected. The transition from the ground state of 1^1A_g is pseudoparity-forbidden because of the alternant symmetry. The polarization (Q_{II}) is parallel to the inner H—H axis. Previous calculated results also give a very weak intensity for the transition.

The second valence excited state is computed to be the 1^1B_{2u} state. The state is predicted to appear at 2.55 eV at the MRMP level with a medium intensity of 0.0143. This is close to the observed peak at 2.38−2.42 eV in the absorption spectrum with the oscillator strength of 0.07.[11] Previous results estimate slightly smaller excitation energies compared to the present result. The state is dominated by singly excited configurations arising from almost degenerate $1 \rightarrow 1'$ and $2 \rightarrow 2'$ excitations. Both transitions occur between a conjugated pair of orbitals and they mix with the same sign. Thus, the 1^1B_{2u} state is an ionic state. The electric transition dipole moment vectors for $1 \rightarrow 1'$ and $2 \rightarrow 2'$ transitions are similar in magnitude and antiparallel in their orientation. Again, the transition dipoles nearly cancel giving rise to the weak absorption. The polarization ($Q_{\perp}$) is perpendicular to the inner H—H axis.

The Q band of FBP consists of two separate transitions. The lower excited state has a covalent character but the higher

excited state has an ionic character. We must stress here that the Q band is relatively weak because of the psuedoparity-forbidden state which arises from the alternancy symmetry.

The third valence excited state is the 2^1B_{3u} state. This is the corresponding plus state of the minus 1^1B_{3u} excited state. The state can be described by the single transitions of $1\rightarrow2'$ and its conjugate. In this case two transitions mix with the same sign. The $1\rightarrow2'$ and $2\rightarrow1'$ transition dipoles are reinforced, resulting in the strong optically allowed absorption in the near UV region. The computed oscillator strength of 1.6104 is the strongest of all the transitions in Q and B bands of FBP. This state is also an ionic state and CASSCF significantly overestimates the transition energy. The CASSCF excitation energy of 5.10 eV is reduced to 3.10 eV by the addition of the dynamic $\sigma-\pi$ polarization effect through MRMP.

Theory predicted the fourth valence excited state to be the 2^1B_{2u}, which occurs at 3.25 eV with the oscillator strength of 1.5310. This state is described by a linear combination of singly excited configurations of $2\rightarrow2'$ and $1\rightarrow1'$. In contrast to the 1^1B_{2u} state, the mixing coefficients are minus. The addition of the dipole moments occurs in this state and the oscillator strength is again very intense.

The B bands of FBP consist of two separate transitions from the ground state to the 2^1B_{3u} and 2^1B_{2u} states. Both states are ionic and the transitions are optically strongly allowed. The present theory predicts that transitions occur at 3.10 and 3.25 eV, which is in good agreement with the observed peaks of 3.13−3.33 eV.[10,11] The splitting of the B bands is computed to be 0.15 eV.

MRMP computed the excitation energies of the Q band of TA-P to be 1.67 eV for the 1^1B_{3u} state and 2.54 eV for the 1^1B_{2u} state. The perturbation does not change the peak position. However, the Q band of TA-P is far more intense than that of FBP; specifically, the oscillator strength of $Q_\perp$ becomes 0.1895. Figure 3 shows a variation of orbital energies of the active orbitals of metal-free and metalloporphyrins. FBP has the nearly degenerate HOMOs and LUMOs. Replacing meso carbon by more electronegative nitrogen stabilizes HOMOs and LUMOs except in the a_u orbital. The a_u orbital remains invariant to the perturbation because the nodal plane is crossing near the meso positions. Thus, HOMOs clearly split into two levels while the LUMOs remain nearly degenerate. The $b_{1u}(2)$ orbital is more stabilized because of to larger amplitudes at meso positions compared to $a_u(1)$. Thus, the lower transition ($1\rightarrow2'$) is more weighted than its conjugate of ($2\rightarrow1'$) in the 1^1B_{3u} state. Similarly the ($1\rightarrow1'$) transition is more weighted than ($2\rightarrow2'$) in the 1^1B_{2u} state. The pairing theorem is no longer satisfied and both transitions of the Q band are significantly intensified. The excited states corresponding to the B band could not be obtained at the MRMP level, and therefore, gaps are left in Table 3(a).

Let us consider the reduced porphyrins. MRMP excitation energies of DH-P are calculated to be 1.77 and 2.42 eV for the 1^1B_2 and 2^1A_1 states, respectively, which shows a reasonable agreement with the experimental result.[11] The lowest excitation to the 1^1B_2 state is somewhat blue-shifted from FBP and the transition to the 2^1A_1 state is red-shifted although the energy shift is rather small. For TH-P these excitations are predicted to occur at 1.43 and 2.92 eV, respectively. Contrary to DH-P, the lowest 1^1B_{3u} transition is significantly red-shifted and the second-lowest 1^1B_{2u} transition is blue-shifted from the corresponding transitions of FBP.

Computed oscillator strengths of $Q_\parallel$ of DH-P and TH-P are 0.0215 and 0.1383, respectively, while the corresponding oscillator strengths of $Q_\perp$ are calculated to be 0.0001 and 0.0218. That is, the lower energy side transition gains intensity at the expense of the upper transition. Figure 3(a) shows that hydrogenation significantly destabilizes $a_u(1)$ and $b_{2g}(1')$ orbitals. Because the two transitions of ($2\rightarrow2'$) and ($1\rightarrow1'$) remain nearly degenerate, the intensity of the transition to the 2^1A_1 (1^1B_{2u}) state of DH-P (TH-P) remains as weak as in FBP. However, the energy of the two transitions ($1\rightarrow2'$) and ($2\rightarrow1'$) becomes increasingly unequal in the reduced porphyrins and the ($1\rightarrow2'$) transition is more heavily weighted than the conjugated ($2\rightarrow1'$) transition in the 1^1B_1 (1^1B_{2u}) state. Thus, the alternant symmetry is broken in the reduced porphyrins yielding the increase of intensity of the lower component of the Q band.

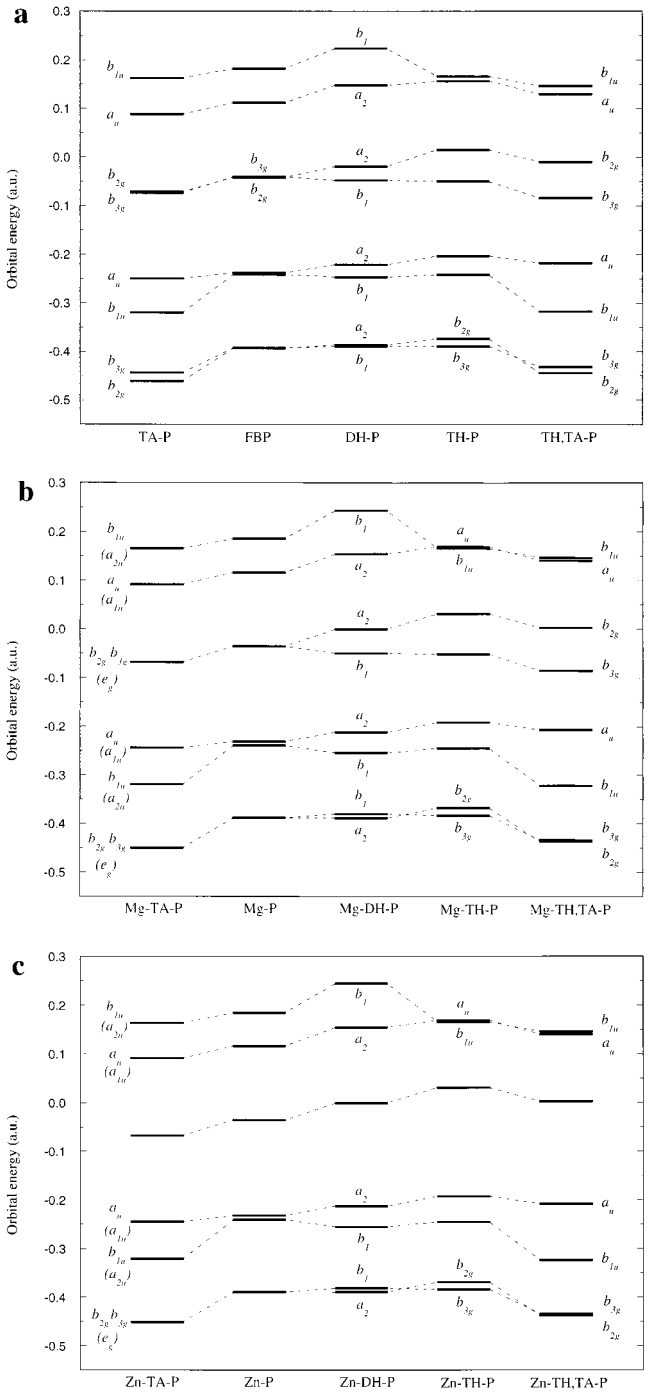

Figure 3. A variation of orbital energies of the active orbitals (four occupied and four unoccupied orbitals) for metal-free porphyrins (a), Mg-porphyrins (b), and Zn-porphyrins (c).

TABLE 3: Singlet Valence $\pi-\pi^*$ Excitation Energies and Oscillator Strength of Porphyrins with 8π Active Electrons in 8π Active Orbitals

(a) Free-base porphyrins

	excitation energy (eV)				oscillator strength		
state	CASSCF	MRMP	exptl.	others	calculated	exptl.	others
TA-P							
1^1B_{3u}	3.07	1.67			0.0970		
1^1B_{2u}	3.62	2.54			0.1895		
2^1B_{3u}	5.50						
2^1B_{2u}	5.54						
FBP							
1^1B_{3u}	2.88	1.63	1.98−2.02[a,b,c]	1.63[d],1.75[e],1.75[f],1.97[g],2.27[h]	0.0026	0.02[b]	0.004[d],0.0007[e],0.0001[f],0.02[h]
1^1B_{2u}	3.53	2.55	2.38−2.42[a,b]	2.11[d],2.40[e],2.23[f],2.40[g],3.42[h]	0.0143	0.07[b]	0.002[d],0.013[e],0.0006[f],0.04[h]
2^1B_{3u}	5.10	3.10	3.13−3.33[a,b]	3.12[d],3.44[e],3.56[f],3.41[g],4.72[h]	1.6104	1.15[b]	0.704[d],0.693[e],1.03[f],1.87[h]
2^1B_{2u}	5.12	3.25		3.08[d],3.47[e],3.75[f],3.24[g],5.29[h]	1.5310		0.911[d],1.20[e],1.73[f],2.55[h]
DH-P							
1^1B_2	2.76	1.77	1.98[b]	2.46[h]	0.0215	0.10[b]	0.10[h]
2^1A_1	3.58	2.42	2.29[b]	3.64[h]	0.0001	0.06[b]	0.02[h]
2^1B_2	4.83	3.19	3.18[b]	5.00[h]	0.7938	0.96[b]	3.36[h]
3^1A_1	5.12	3.43		5.28[h]	1.0838		2.65[h]
TH-P							
1^1B_{3u}	2.76	1.43			0.1383		
1^1B_{2u}	3.80	2.92			0.0218		
2^1B_{3u}	5.52	3.66			1.5938		
2^1B_{2u}	5.41	3.68			1.4775		
TH,TA-P							
1^1B_{3u}	2.80	1.35			0.2305		
1^1B_{2u}	4.04	3.06			0.0431		
2^1B_{2u}	5.61	3.57			1.2731		
2^1B_{3u}	6.14	3.88			1.2895		

(b) Mg-porphyrins

	excitation energy (eV)				oscillator strength	
state	CASSCF	MRMP	exptl.	others	calculated	others
Mg-TA-P						
1^1E_{1u}	3.30	2.02			0.1544	
2^1E_{1u}	5.53	3.06			1.2146	
Mg-P						
1^1E_{1u}	3.16	2.00	2.17[i]	2.01[j]	0.0106	0.0015[j]
2^1E_{1u}	5.04	3.07	3.09[i]	3.63[j]	1.5613	1.99[j]
Mg-DH-P						
1^1B_2	3.26	1.98			0.1114	
2^1A_1	3.15	2.10			0.0091	
2^1B_2	4.89	3.04			0.8231	
3^1A_1	4.61	3.28			0.6463	
Mg-TH-P						
1^1B_{3u}	2.82	1.50			0.2274	
1^1B_{2u}	3.48	2.39			0.0236	
2^1B_{2u}	5.31	3.39			1.3611	
2^1B_{3u}	5.55	3.56			1.2710	
Mg-TH,TA-P						
1^1B_{3u}	2.90	1.46			0.2959	
1^1B_{2u}	3.81	2.62			0.0324	
2^1B_{2u}	5.58	3.39			1.2242	
2^1B_{3u}	6.30	3.94			1.0376	

(c) Zn-porphyrins

	excitation energy (eV)			oscillator strength	
state	CASSCF	MRMP	exptl.	calculated	exptl.
Zn-TA-P					
1^1E_{1u}	3.32	2.13	2.13[l]	0.1666	
2^1E_{1u}	5.57	3.30	3.44[l]	1.3047	
Zn-P					
1^1E_{1u}	3.18	2.11	2.21[i],2.18[k]	0.0121	0.005[k]
2^1E_{1u}	5.06	3.21	3.09[i],3.13[k]	1.6281	0.98[k]
Zn-DH-P					
1^1B_2	3.26	1.99	2.04[k]	0.1114	0.06[k]
2^1A_1	3.17	2.15	2.33[k]	0.0096	0.007[k]
2^1B_2	4.92	3.06	3.29[k]	0.8231	
3^1A_1	4.63	3.33	3.13[k]	0.6463	

TABLE 3 (Continued)

(c) Zn-porphyrins

state	excitation energy (eV)			oscillator strength	
	CASSCF	MRMP	exptl.	calculated	exptl.
Zn-TH-P					
1^1B_{3u}	2.82	1.56		0.2310	
1^1B_{2u}	3.54	2.54		0.0226	
2^1B_{2u}	5.34	3.50		1.4193	
2^1B_{3u}	5.58	3.69		1.3297	
Zn-TH,TA-P					
1^1B_{3u}	2.91	1.54		0.3105	
1^1B_{2u}	3.85	2.78		0.0388	
2^1B_{2u}	5.62	3.55		1.2895	
2^1B_{3u}	6.35	4.14		1.1055	

[a] 1.98 eV in the gas phase, 2.01 eV in C_6H_6, and 2.02 eV in C_2H_5OH for 1^1B_{3u} state, 2.38 eV in C_6H_6, 2.39 eV in C_2H_5OH, and 2.42 eV in the gas phase for 1^1B_{2u} state, 3.13 eV in C_6H_6, 3.17 eV in C_2H_5OH, and 3.33 eV of the vapor optical spectra for B band; ref 10. [b] 2.02 eV for 1^1B_{3u} state, 2.39 eV for 1^1B_{2u} state, 3.15 eV for B band in C_6H_6, and in C_6H_6 for DH-P; ref 11. [c] 1.98 eV in anthracene; ref 12. [d] CASPT2; ref 18. [e] STEOM-CCSD; ref 20. [f] SAC-CI; ref 19. [g] MRSD$\sigma\pi$CI; ref 17. [h] MRSDπCI; ref 11. [i] In $CHCl_3$; ref 13. [j] SAC-CI; ref 19. [k] In CH_3OH; ref 14. [l] In $CHCl_3$-CH_3OH; ref 15.

The B bands of DH-P are computed to appear at 3.19 and 3.43 eV with the oscillator strengths of 0.7938 and 1.0838, respectively. The excitation energies and intensities show a good agreement with the observed value of 3.18 eV with the intensity of 0.96.[11] MRSDπCI[11] overestimates the excitation energy and intensity due to the lack of σ-electron effects. MRMP placed the intensities 2^1B_{3u} and 2^1B_{2u} of TH-P at 3.66 and 3.68 eV, respectively. Both transitions are calculated to be somewhat blue-shifted from FBP.

The effects on the wavelengths and absorption strengths of the Q band are enhanced if TA-P is hydrogenated. The Q band of TH,TA-P is computed to occur at 1.35 eV for the 1^1B_{3u} state and at 3.06 eV for the 1^1B_{2u} state. The computed oscillator strength goes up to 0.2305 for the transition to the 1^1B_{3u} state, whereas the transition to the 1^1B_{2u} state has an intermediate intensity. We see that the lowest 1^1B_{3u} state is red-shifted and intensified and the second-lowest 1^1B_{2u} band is blue-shifted and also intensified compared to those of TH-P. The strong B band of TH,TA-P is predicted to appear at 3.57 and 3.88 eV, respectively, which is significantly blue-shifted from FBP.

The Q and B Bands of Mg and Zn Porphyrins. Let us consider the effects of the central substituent on the Q and B bands. Table 3(b) shows the calculated results of Mg-P. CASSCF overestimates the excitation energies and MRMP again represents a great improvement over CASSCF. Mg-P has the D_{4h} symmetry of full point group and the two states of the Q band are degenerate with the $^1E_{1u}$ symmetry. The MRMP excitation energy of 2.00 eV to the 1^1E_{1u} state of Mg-P is close to the mean value of the two separate transitions of FBP. The calculated value is also close to the observed peak at 2.17 eV in the absorption spectrum in CH_3Cl.[13] SAC-CI[19] also yields 2.01 eV, which is very close to our value. The $1^1E_{1u}(^1B_{3u})$ state is well-described mainly by singly excited $\pi\rightarrow\pi^*$ transitions of $1\rightarrow2'$ and $2\rightarrow1'$, which have nearly the same weight with a different sign, and the $1^1E_{1u}(^1B_{2u})$ state is represented by $1\rightarrow1'$ and $2\rightarrow2'$ transitions with a same sign. Introduction of Mg atom in the center of a molecule enforces the two LUMOs of b_{2g} and b_{3g} to be degenerate and there is little change in the intensity of the Q band. That is, the transition is pseudoparity-forbidden and the computed intensity is still weak with the oscillator strength of 0.0106. The excitation energy to the second 2^1E_{1u} state is calculated to be 3.07 eV, which is in good agreement with the experimental value of 3.09 eV.[13] SAC-CI[19] placed the 2^1E_{1u} state at a somewhat higher position. The transition to the 2^1E_{1u} state is optically allowed and the calculated oscillator strength is 1.5613.

The excitation energies to the 1^1E_{1u} and 2^1E_{1u} states of Mg TA-P are computed at 2.02 and 3.06 eV, respectively. These transition energies are very close to those of Mg-P. That is, substitution of nitrogen atoms for carbon atoms in meso position has little effect on the position of Q and B bands. However, the intensity of the Q band is significantly intensified. The computed oscillator strength to the transition to the 1^1E_{1u} state is 0.1544, which is slightly smaller than the stronger 1^1B_{2u} transition of metal-free TA-P. Figure 3(b) shows that the b_{1u} (2) orbital of Mg-TA-P is significantly stabilized relative to the other orbitals. Thus, the energy of the two conjugated transitions becomes increasingly unequal and the lower energy transition from b_{1u} is more heavily weighted than the other conjugated transition, leading to the increase of intensity of the Q band. Conversely, the oscillator strength of the B band becomes slightly weaker compared to that of Mg-P, although it is still intense.

Because of the breakdown of the degeneracy, the Q band of Mg-DH-P splits into two separated peaks. They are placed at 1.98 ($^1B_2$) and 2.10 eV ($^1A_1$). The lower transition becomes 10 times stronger than the corresponding 1^1E_{1u} transition of Mg-P but the upper transition becomes significantly weak because of the psuedoparity. The lower Q band gains intensity at the expense of the upper Q band.

Calculated excitation energies of Mg-TH-P are 1.50 eV for 1^1B_{3u} state and 2.39 eV for 1^1B_{2u} state. The splitting width of two separate peaks spreads to 0.89 eV. The lower state moves to the red by 0.50 eV and the higher state moves to the blue by 0.39 eV from Mg-P. Computed oscillator strength is 0.2274 and 0.0236 for the transitions to the 1^1B_{3u} and 1^1B_{2u} states, respectively. Mg-TH-P has much stronger intensity than Mg-P and metal-free TH-P. When compared with the metal-free TH-P, the mixing weight of the two transitions becomes more unequal, which leads to the increase of intensity. The B bands are located at 3.39 and 3.56 eV with strong intensity. Both transitions are blue-shifted from the corresponding transitions of Mg-P.

The Q band of Mg-TH,TA-P is computed to occur at 1.46 eV (0.2959) for the 1^1B_{3u} state and at 2.62 eV (0.0324) for the 1^1B_{2u} state. Values in parentheses are the calculated oscillator strength. The Q band becomes more intense than that of Mg-TH-P. Thus, hydrogenation splits the degenerate Q band of Mg-TA-P equally into two peaks. However, the B band is significantly blue-shifted and the peaks are computed to appear at 3.39 and 3.94 eV, respectively.

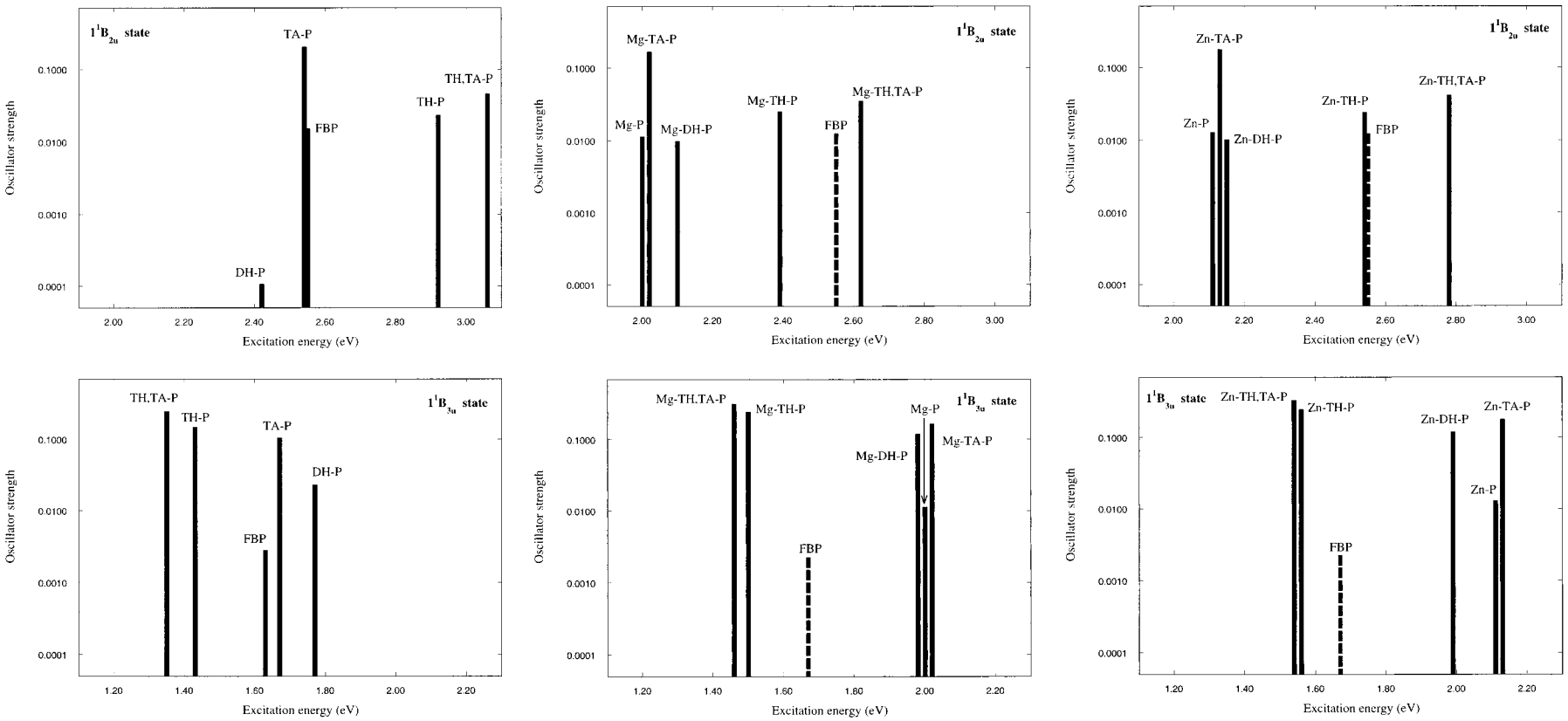

Figure 4. MRMP excitation energies and oscillator strengths of the Q band of metal-free porphyrins (a), Mg-porphyrins (b), and Zn-porphyrins (c).

The excitation energies and oscillator strength of Zn-P are summarized in Table 3(c). The spectra of the Q and B bands of Zn-P have the same tendency as those of Mg-P. The MRMP 1^1E_{1u} and 2^1E_{1u} excitation energies are 2.11 and 3.21 eV, in good agreement with the observed values.[13] The reasonable agreement between theory and experiment is also found in the Q and B bands of Zn-TA-P[15] and Zn-DH-P.[14] Although there is little difference between Mg-P and Zn-P compounds, the Q band of the latter moves to the blue by 0.01−0.16 eV from the Mg compounds and the B band is blue-shifted by 0.02−0.24 eV. Calculated oscillator strength of Zn-P is slightly stronger than the corresponding intensity of Mg-P. The minimum shift is again found in dihydro derivatives. As a result, Mg-DH-P and Zn-DH-P have very similar Q and B bands.

Effects of Chemical Modification on Optical Spectra. The optical spectra, particularly the Q band of porphyrins, are perturbed to a greater or lesser extent by various chemical modifications to the basic FBP. Figure 4 summarizes the Q band of various porphyrins. Generally speaking, insertion of aza groups increases the intensity of the higher component of the Q band without changing the peak position. Hydrogenation widens the splitting of the two peaks and intensifies the lower component at the expense of the higher component.

The relative order for the lowest 1^1B_{3u} state of metal-free porphyrins is TH,TA-P < TH-P < FBP, TA-P < DH-P. The resulting order for the second excited 1^1B_{2u} state is just the reverse, that is, TH,TA-P > TH-P > FBP, TA-P > DH-P. Hydrogenation leads to the red-shift for the lowest 1^1B_{3u} state whereas the 1^1B_{2u} state moves to the blue by the perturbation. The insertion of aza groups has little effect on the peak position of the Q band although peaks are slightly red-shifted. Thus, the Q bands of FBP and TA-P are expected to appear almost at the same position. This is true for the metalloporphyrins. These chemical modifications to the basic structure of FBP break the pairing properties and the intensity of the Q band becomes stronger.

The hydrogenation and insertion of aza groups to Mg-P and Zn-P have a similar tendency as that for metal-free porphyrins. That is, hydrogenation of metalloporphyrins leads to the splitting of the degenerate Q band, giving rise to the red-shift for the lowest 1^1B_{3u} states and the blue-shift for the second-lowest 1^1B_{2u} states. However, the splitting widths of the two states of the Q band of reduced metalloporphyrins are smaller than those of corresponding metal-free reduced porphyrins. The insertion of aza groups has little effect to the position of the Q band. The metalloporphyrins have similar intensity variations as those of metal-free porphyrins.

Figure 5 summarizes the Q band with medium and strong intensity of various porphyrins treated here. Comparing metal-free and metalloporphyrins, we see that the ordering of the lowest 1^1B_{3u} state is metal-free < Mg-P < Zn-P. The intensity increases in the same order. The ordering for the second excited 1^1B_{2u} state is Mg-P < Zn-P < metal-free. The intensity increases again in the same order. These characteristics are common to all the porphyrin derivatives.

The two intense B bands of FBP appear at 3.10 and 3.25 eV in the near-UV and UV region. DH-P slightly shifts the peak position to the blue (0.1−0.2 eV) and weakens the intensity. Considerable blue-shift is observed in the B band of TH-P and TH,TA-P. In particular, the higher component moves significantly to the blue. However, the intensity decreases slightly although it is still very strong. As a result, the strongest intensity is produced in FBP. Metalloporphyrins show a similar tendency. The most intense band is found in unperturbed Mg-P and Zn-P. TH and TH,TA modifications yield the significant blue-shift, whereas TA and DH metalloporphyrins do not change the peak position. Although there is little difference between Zn-P and Mg-P, the B band of Zn-P moves more to the blue than that of Mg-P.

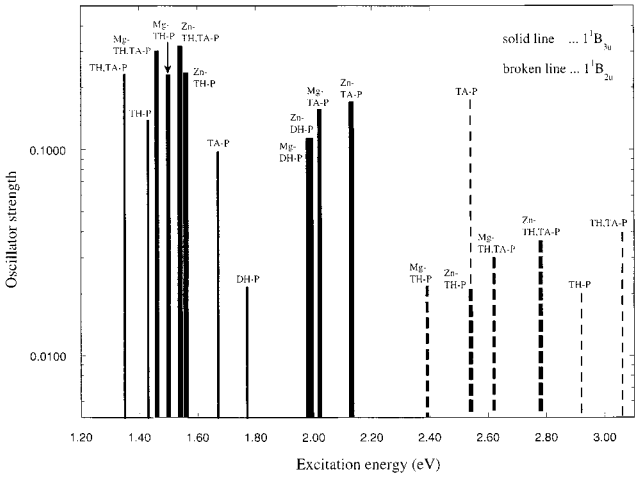

Figure 5. Summary of the MRMP Q band of various porphyrins. Absorption with strong or medium intensity is shown.

4. Summary

In this work, MRMP was applied to the study of the Q and B bands of FBP, Mg-P, and Zn-P, and their derivatives. The weakness of the Q band of FBP is due to pseudoparity-forbidden status that originated from the pairing properties of alternant hydrocarbons. The Q band intensity can be strengthened if the pairing properties are broken. This is achieved by substituting nitrogen atoms for carbon atoms in meso position, breaking π conjugation by hydrogen addition to one or two pyrrole rings, and introducing Mg and/or Zn atom in the center of molecule. A number of features can be extracted from this study.

(1) The chemical modifications produce the change of the macrocyclic porphyrin skeleton. Insertion of aza groups in meso position and hydrogenation have the opposite effects on the size of the central hole. The former shrinks the central hole but the latter expands it. The Mg and Zn substitution has little effect on the geometrical changes.

(2) Substituting nitrogen atoms for meso carbon atoms significantly intensifies the oscillator strength of the higher component of the Q band, but the perturbation has little influence on the peak position. Consequently, the Q bands of FBP and TA-P are expected to appear almost at the same wavelength. This is true for the metalloporphyrins.

(3) Ring reduction widens the splitting of two peaks of the Q band. That is, hydrogenation makes the lower component of the Q band shift to the red and the higher component shift to the blue, yielding the characteristically strong far-red band due to $1^1A_g \rightarrow 1^1B_{3u}$ and the weak visible band due to $1^1A_g \rightarrow 1^1B_{2u}$.

(4) These effects are enhanced in TH,TA-P by substituting nitrogen atoms for carbon atoms in meso position and by hydrogen addition to pyrrole rings. TH,TA-P produces the intense far-red band and the visible band with medium intensity.

(5) Changes from metal-free to metallocomplexes have a less dramatic effect on the spectra. We found that the ordering of the lowest 1^1B_{3u} state and the second lowest 1^1B_{2u} state is 1^1B_{3u}: metal-free < Mg-P < Zn-P; 1^1B_{2u}: Mg-P < Zn-P < metal-free. The intensity increases in the same order. These characteristics are common to all the porphyrin derivatives.

Figure 5 provides useful information about how to control the intensity and color of the Q band of the porphyrin compounds in the visible region.

Acknowledgment. The present research was supported in part by a grant-in-aid from the Ministry of Education, Science, Sports, and Culture. The computations were carried out on an IBM SP2 system at the Intelligent Modeling Laboratory (IML) of the University of Tokyo. The CASSCF reference wave functions were obtained using a MOLPRO program.[21] The perturbation calculations were performed with an MR2D program.[22]

References and Notes

(1) Gouterman, M. *J. Chem. Phys.* **1959**, *30*, 1139.

(2) (a) Hashimoto, T.; Nakano, H.; Hirao, K. *J. Chem. Phys.* **1996**, *104*, 6244. (b) Kawashima, Y.; Hashimoto, T.; Nakano, H.; Hirao, K. *Theor. Chem. Acc. (Fukui Memorial Issue)* **1998**, in press.

(3) Almlof, J.; Fischer, T. H.; Gassman, P. G.; Ghosh, A.; Haser, M. *J. Phys. Chem.* **1993**, *97*, 10964.

(4) Dunning, T. H. *J. Chem. Phys.* **1989**, *90*, 1007.

(5) Huzinaga, S.; Andzelm, J.; Klobukowski, M.; Radzio-Andzelm, E.; Sakai, Y.; Tatewaki, H. *Gaussian Basis Set for Molecular Calculation;* Elsevier: New York, 1984.

(6) (a) Siegbahn, P. E.; Heiberg, A.; Roos, B. O.; Levy, B. *Phys. Scr.* **1980**, *21*, 323. (b) Roos, B. O.; Taylor, P. R.; Siegbahn, P. E. *Chem. Phys.* **1980**, *48*, 157. (c) Roos, B. O. *Int. J. Quantum Chem.* **1980**, *S14*, 175.

(7) Hirao, K. *Chem. Phys. Lett.* **1992**, *190*, 374; **1992**, *196*, 397; **1993**, *201*, 59; *Int. J. Quantum Chem.* **1992**, *S26*, 517.

(8) Chen B. M. L.; Tulinsky, A. *J. Am. Chem. Soc.* **1972**, *94*, 4144.

(9) Ghosh, A. *J. Phys. Chem. B* **1997,** *101*, 3290.

(10) Edwards, L.; Dolphin, D. H.; Gouterman, M.; Adler, A. D. *J. Mol. Spectrosc.* **1971**, *38*, 16.

(11) Nagashima, U.; Takada, T.; Ohno, K. *J. Chem. Phys.* **1986**, *85*, 4524.

(12) Kim, B. F.; Bohandy, J. *J. Mol. Spectrosc.* **1978**, *73*, 332.

(13) Dolphin, D. *The porphyrins*; Academic Press: New York, NY, 1978; Vol. III.

(14) Sekino, H.; Kobayashi, H. *J. Chem. Phys.* **1987**, *86*, 5045.

(15) Dvornikov, S. S.; Knyukshto, V. N.; Kuzmitsky, V. A.; Shulga, A. M.; Solovyov, K. N. *J. Lumin.* **1981**, *23*, 373.

(16) Foresman, J. B.; Head-Gordon, M.; Pople, J. A.; Frisch, M. J. *J. Phys. Chem.* **1992**, *96*, 135.

(17) Yamamoto, Y.; Noro, T.; Ohno, K. *Int. J. Quantum Chem.* **1992**, *42*, 1563.

(18) (a) Serrano-Andres, L; Merchan, M.; Rubio, M.; Roos, B. O. *Chem. Phys. Lett.* **1998**, *295*, 195. (b) Merchan, M.; Orti, E.; Roos, B. O. *Chem. Phys. Lett.* **1994**, *226*, 237.

(19) (a) Nakatsuji, H.; Hasegawa, J.; Hada, M. *J. Chem. Phys.* **1996**, *104*, 2321. (a) Hasegawa, J.; Hada, M.; Nonoguchi, M.; Nakatsuji, H. *Chem. Phys. Lett.* **1996**, *250*, 159.

(20) Gwaltney S. R.; Bartlett, R. J. *J. Chem. Phys.* **1998**, *108*, 6790.

(21) MOLPRO is a package of ab initio programs written by Werner, H. J.; Knowles, P. J. with contributions from Almlof, J.; Amos, R. D.; Deegan, M. J. O.; Elbert, S. T.; Hampel, C.; Meyer, W.; Peterson, K.; Pitzer, R.; Stone, A. J.; Taylor, P. R.; Lindh, R.

(22) (a) Nakano, H. *J. Chem. Phys.* **1993**, *99*, 7983. (b) MR2D Ver. 2, Nakano, H. University of Tokyo, 1995.